Thermal Modeling of Inductor and Transformer Windings Including Litz Wire

Phyo Aung Kyaw, Mylene Delhommais, Jizheng Qiu, Charles R. Sullivan, Jean-Luc Schanen, Cecile Rigaud

Thermal Modeling of Inductor and Transformer Windings Including Litz Wire

Phyo Aung Kyaw, *Student Member, IEEE*, Mylène Delhommais, *Student Member, IEEE*, Jizheng Qiu, Charles R. Sullivan, *Fellow, IEEE*, Jean-Luc Schanen, *Senior Member, IEEE* and Cécile Rigaud

***Abstract*—Design optimization of magnetic components which considers both electrical and thermal performance can help in designing power converters with a high power density. This paper proposes an approximate analytical model for thermal resistance of inductor and transformer windings, including litz wire, which only requires knowledge of thermal properties of constituent materials and geometric dimensions. The model is based on regular square and hexagonal packing of insulated wires, and is derived by integration of infinitesimal thermal resistances along specified heat flow path. The model closely agrees with finite element analysis (FEA) and can be used in place of time-consuming FEA as part of larger thermal network models for magnetic components. The model is also experimentally validated using a toroidal inductor with a litz-wire winding; the model has less than 12% error compared to the experimental measurement. Application of the model for practical windings, including litz-wire windings, is also discussed. The model can be used during the design process of magnetic components of a switching power converter to evaluate the temperature and potential hot spots. The model provides closed-form results, hence fast computation times, and so can be used in design optimization procedures.**

***Index Terms*—temperature measurement, windings, inductors, transformers**

I. Introduction

Nowadays, with the emergence of electric vehicles and aircraft, static power converter designers face the challenge of volume or weight reduction. Recent advances in wide bandgap semiconductors allow for efficient high-frequency switching, and magnetics such as inductors and transformers increasingly dominate the size and loss of switching power converters [1], [2]. Magnetic components are usually custom designed for minimum loss under application specific efficiency or size constraints.

For designing magnetics, optimization procedures which consider both losses and thermal performance, such as that in [3] for a buck converter, are desirable since losses in magnetic cores and windings are temperature dependent. Such optimization procedures require analytical models with fast computation times for losses and heat flow inside the component. Thermal modeling of windings is usually challenging because of the round-wire shape and the combination of different materials such as copper, insulator, and air or resin between each wire. Modeling the thermal performance of windings made of litz wire is especially important because litz wire has poor effective thermal conductivity as a result of its individually insulated fine wire strands.

It is possible to find in the literature, analytical thermal models of inductor and transformer windings. A 2D thermal equivalent model is proposed in [4] for a toroidal transformer made of several layers of round wire but is not applicable to litz-wire strands that are randomly distributed. The analytical model in [5] provides a formula for thermal conductivity of impregnated litz wire with different strand shapes, but requires tuning and calibration using experimental data to correctly predict the thermal transfer. The model in [6] only requires physical and geometrical description, but has an error of around 50% for litz wire. The thermal conductivity of litz wire can be experimentally identified as discussed in [7], but the measured results are only applicable for the specific litz wire used in the experiment.

This paper presents an approximate analytical thermal model for windings made of solid magnet wire or litz wire [8], and is verified experimentally using the method presented in [7]. Application of the model for practical windings and as part of larger thermal network models for magnetic components is also discussed in details. Section II describes thermal network modeling of magnetic components using a toroidal inductor as an example. An approximate analytical formula for effective thermal resistance of individually insulated wire strands is proposed in Section III. The proposed model is verified in Section IV by comparing it with finite element analysis. Section V discusses application of the proposed analytical model in practical windings and litz wire. Section VI describes experimental verification of the proposed model in toroidal inductor samples. The experiment shows that the effective thermal conductivity across litz wire can be calculated with an error less than 12% using the proposed model.

II. Thermal Network Modeling of Magnetics

Thermal modeling of magnetics involves calculating the temperature at various locations inside inductors or transformers, and is usually performed to verify that the component remains below a specified maximum temperature and to determine adequate cooling systems. For simple cases such as a single loop of wire, temperatures can be calculated by solving the heat equation. For typical inductors and transformers in power converters, which usually comprise multiple materials and in which heat generation is distributed, finite element

This work was supported partly by the National Science Foundation under Grant 1610719.

Phyo Aung Kyaw and Charles R. Sullivan are with Thayer School of Engineering at Dartmouth, Hanover, NH 03755, USA (e-mail: phyo.aung.kyaw@dartmouth.edu).

Mylène Delhommais and Jean-Luc Schanen are with Univ. Grenoble Alpes, CNRS, Grenoble INP, G2Elab, F-38000 Grenoble, France.

Jizheng Qiu is with Tesla, Inc., Palo Alto, CA 94304, USA.

Cécile Rigaud is with Tronico, 38000 Grenoble, France.

Color versions of one or more of the figures in this paper available online at https://ieeexplore.ieee.org.

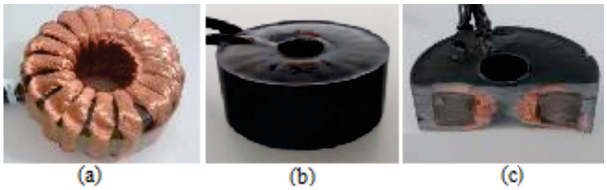

Fig. 1. The studied toroidal inductor. (a) Inductor without resin, (b) molded inductor, and (c) cross-section showing the inside of the molded inductor.

analysis (FEA) can be used to obtain temperatures at various locations inside the component. However, FEA is usually time-consuming and not useful for design optimization.

A. Thermal Network Modeling Principle

Thermal network modeling is a first order method for calculating temperatures at certain points inside a component. The heat generated and thermal capacitance of different parts of the component are nodalized with respect to geometry and internal hot spots, and different nodes are connected with thermal resistors. Thermal network modeling is approximately similar to FEA, but with orders-of-magnitude fewer nodes, resulting in faster computation times. The thermal network can be solved using typical circuit analysis techniques. The minimum number of nodes required depends on the symmetry, homogeneity and isotropy of the component, and the number of nodes can be chosen based on the trade-off between accuracy and computation time.

B. Toroidal Inductor Example

A sample toroidal inductor (Fig. 1) used for thermal modeling in this paper is described in Table I. The inductor is designed to be used in an interleaved buck converter which will be placed in the stratosphere. The air pressure at this altitude is about 7% of the atmospheric pressure at the sea level, and so the power electronics components can only be cooled using a cold plate. The winding is made of litz wire to limit ac copper losses. The inductor is molded into a resin for safety reasons in order to withstand 3 kV between the litz wire and the converter case, and for better thermal conduction of heat generated inside the inductor core to the cold plate.

Due to the azimuthal symmetry of the toroidal inductor, a 2D thermal network model (Fig. 2) is sufficient for accurate modeling. The level of discretization depends on the designer's choice and application specifications. In Fig. 2, the core loss is split into 4 different nodes, as is the winding loss. The winding, made of litz wire, is considered to be orthotropic whereas the other materials (magnetic core, epoxy, resin) are considered to be isotropic.

C. Requirements for the Thermal Network Model

Calculating the temperatures at various nodes in the thermal network model (Fig. 2) for a particular heat sink temperature T_{heatsink} requires knowledge of the values of all thermal resistors. This requires the thermal conductivity of all materials of the sample inductor as well as various dimensions. For the magnetic core, the epoxy resin coated on the core and the resin molding the inductor, the thermal properties are

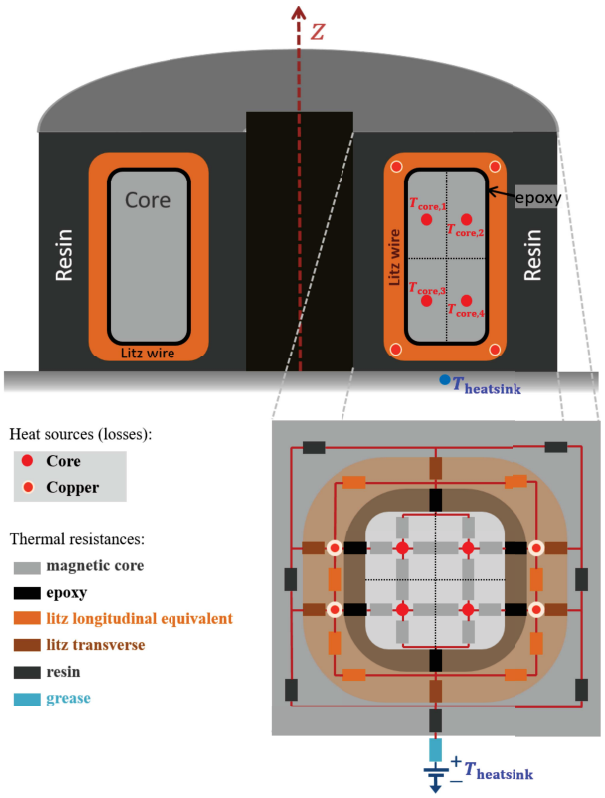

Fig. 2. Two-dimensional thermal network model of the sample inductor.

independent of the design parameters and dimensions, and can be obtained from the manufacturer or from experimental measurements [7]. The effective thermal properties of the litz-wire winding, which comprises copper, insulator and enamel insulation coating, as well as inductor molding resin and some air confined between the strands, depend on the particular inductor designs.

An analytical model for the effective thermal conductivity of litz-wire windings, which can be calculated from the thermal properties of the constituent materials is required for the thermal network model. In this paper, we presents an analytical model for calculating the effective thermal resistance and conductivity of inductor and transformer windings and litz wire which only requires the knowledge of thermal properties of the constituent materials and various dimensions. The accuracy of this model for regularly packed wires is tested using finite element analysis and its applicability for practical inductor windings is also experimentally verified.

III. Thermal Model for Insulated Round Wires

This section presents an approximate analytical thermal model for calculating the effective thermal conductivity and resistance of a group of insulated round wire strands. The model is to be used in a thermal network model as described in Section II, which accounts for the directions of heat flow. It can also be used in other thermal models or finite element analysis which model the winding region as a single material omitting the detailed strand structure.

The group of insulated wires can represent either inductor and transformer windings or litz wire. The combination of

TABLE I
INDUCTOR SPECIFICATIONS

Data	Parameters
Geometry	Toroidal. (d_{out}: 62.91 mm, d_{in}: 31.69 mm, h: 25.91 mm)
Core material	powder (KoolMu), k_{core} = 3.95 W/(m · K), k_{epoxy} = 0.34 W/(m · K)
Molding material	Epoxy Resin 50-3100, k_{resin} = 2.16 W/(m · K)
Winding	litz wire, modified polyurethane enamel coating k_{ins} = 0.028 W/(m · K), no outer insulation

the wire conductor material, the insulation layer around it and the gap between the wires is defined in this paper as one level of insulation. By this definition, litz-wire windings have two levels of insulation: the first (strand) level consists of the individual strands with the enamel insulation coating and the gap between the strands; and the second (winding) level comprises the twisted bundles with the outer insulation layer and the gap between the winding turns.

Anisotropy of thermal properties requires that the model provides the effective thermal conductivity and resistance for two distinct directions: along the length of the wire (longitudinal) and across the diameter of the wire (transverse). This paper focuses on the transverse conduction since the longitudinal thermal resistance is a simple parallel combination of the thermal resistance of various constituent materials.

In the following equations, R represents thermal resistance, dR infinitesimal thermal resistance, k thermal conductivity, l length and t thickness. For the subscripts, c refers to the conductor, ins the wire insulation, hl the horizontal insulation layer (Fig. 3), vl the vertical insulation layer (Fig. 3), g the gap between wires, l the longitudinal direction along the length of the wire, t the transverse direction across the diameter of the wire and int integration.

A. Longitudinal Thermal Resistance

The effective longitudinal thermal resistance R_l, along the length of the wire, for one level of insulation, can be modeled as a parallel combination of thermal resistance of various materials in the wire:

$$R_l = \left(\sum_{\text{mat}} \frac{1}{R_{\text{mat},l}} \right)^{-1}, \tag{1}$$

where the subscript mat refers to various materials, such as the conductor, insulation coating on each wire, gap between the wires and the horizontal and vertical insulation layers, and $R_{\text{mat},l}$ is the longitudinal thermal resistance of these materials. Substituting $l/(kA)$ for thermal resistance, where k is thermal conductivity, l length and A cross-sectional area gives the effective longitudinal thermal conductivity

$$k_l = \frac{1}{A_l} \sum_{\text{mat}} k_{\text{mat},l} A_{\text{mat},l}, \tag{2}$$

where A_l is the total cross-sectional area of all materials in the group of insulated wires, and $k_{\text{mat},l}$ and $A_{\text{mat},l}$ are respectively the thermal conductivity and cross-sectional area of each material. The effective longitudinal thermal conductivity k_l is simply an area-weighted combination of the thermal conductivities of various materials in the wire, regardless of the particular packing structure of the wires.

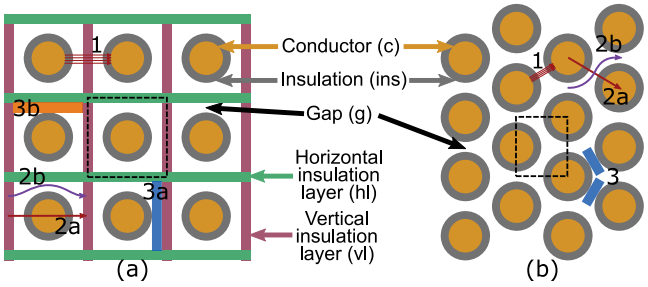

Fig. 3. Cross-section of (a) square-packed, (b) hexagonal-packed wires with one level of insulation, showing conductive material (c), insulation coating (ins) and gap (g). The horizontal insulation layer (hl) and the vertical insulation layer (vl) represent insulation tape often used in windings, and both are displayed for the purpose of developing the thermal model for square-packed wires; wires in practice will include none or only one type of layer. The figure is not drawn to scale; in practice, the insulation is usually much thinner than the conductor diameter and separation between wires is also relatively much smaller. The black dashed boxes represent unit cells of the wires. It is assumed that heat flows from left to right in each packing.

B. Transverse Thermal Resistance: Model Overview

The transverse thermal resistance, for heat flow across the diameter of the wire, however, is not a simple series combination of thermal resistance of various materials. The most accurate method to calculate the transverse thermal resistance is to perform a finite element analysis (FEA) which can be time-consuming. Various analytical models exist for calculating the transverse thermal resistance, and one of the more accurate models draw an analogy between heat flow and electrostatic field [6], which will be refered to in this paper as the Thermal-Electrostatic Field Analogy (TEFA) model.

Because of the similarity between direction of heat flow and electric field lines between two insulated round wires, an analogy can be drawn between the two phenomena. Heat flow is analogous to charge, thermal conductance to capacitance, temperature difference to voltage and thermal conductivity to permittivity. Thus, the thermal resistance between two insulated round wires can be calculated using the equations for the capacitance between two insulated round wires. The TEFA model assumes that the wires are arranged in square or hexagonal packing (Fig. 3) and the capacitance is calculated assuming particular configuration for electric field within each material in the winding. This TEFA model has an error of around 20% for solid wire windings and 50% for litz-wire windings [6].

This paper proposes a more general analytical approach to the TEFA model in [6]. It can be shown that the proposed model and the TEFA model provide similar results if the wires are touching one another with the exception of a vertical insulation layer in square-packed wires; if the gap material between wires is air ($k_g = k_{\text{air}}$); and if the conductor thermal

conductivity k_c is infinite [8]. First, the impacts of finite k_c, separation between wires along the direction of heat flow (blue strips labeled 3a in Fig. 3 (a) and 3 in Fig. 3 (b)) and the horizontal insulation layer are added to the TEFA model using $R = l/(kA)$ for different materials. This extended version of the TEFA model provides the thermal resistance for heat flowing through the wires (red arrows labeled 2a in Fig. 3).

The proposed model combines the extended TEFA model with a thermal resistance model for heat flow in the gap around the wires (purple arrows labeled 2b in Fig. 3). If the gap thermal conductivity k_g is very low, the thermal resistance for heat flowing around the wires will be high; in this case, heat will mainly flow through the wires (red arrows labeled 2a in Fig. 3) and the extended TEFA model approximates the effective thermal resistance R_{eff}. For very high k_g, however, heat will mainly flow around the wires (purple arrows labeled 2b in Fig. 3) and the gap thermal resistance model for heat flow around the wires approximates R_{eff}. Thus, we propose that R_{eff} can be modeled as a parallel combination of these two thermal resistance models.

The parallel combination, however, is only approximate based on the asymptotic behavior of R_{eff} for very low and very high k_c. For intermediate values of k_c, heat flows both through and around the wires. Because there is an overlap in the regions of the gap modeled by the two thermal resistance models (2a and 2b in Fig. 3), the parallel combination results in double counting of thermal conductance of some portion of the gap. However, as will be discussed below, this double-counting effect only introduces less than 15% error, and so R_{eff} is approximated as a parallel combination of the extended TEFA model and the gap thermal resistance model.

The proposed model considers square-packed and hexagonal-packed wires as shown in Fig. 3, similar to the TEFA model. An arbitrary random packing in practical windings and litz wire can be considered as some weighted combination of local square and hexagonal packing. The effective thermal resistance is derived by assuming particular heat flow directions (red enclosed areas in Figs. 4 and 5) and integrating infinitesimal thermal resistance along these directions; this is similar to the assumption for electric field lines in the TEFA model [6].

C. Transverse Thermal Resistance: Square-Packed Wires

The transverse thermal resistance of a unit cell of square-packed wires R_{sq} is equal to that of the quarter-unit cell shown in Fig. 4; a unit cell comprises four quarter-unit cells in a 2×2 configuration that forms a complete wire as shown in Fig. 3 (a). R_{sq} is a parallel combination of three thermal resistances – 1) across the wire and through the gap towards the dark pink vertical layer $R_{\theta,\text{int}}$ (red arrow labeled 2a in Fig. 3 (a) and integral of dR_θ in Fig. 4 (a)); 2) across the green horizontal layer R_{hl}; and 3) across the gap around the wire R_g (purple arrow labeled 2b in Fig. 3 (a) and integral of dR_g in Fig. 4 (b)) – and can be written as

$$\frac{1}{R_{\text{sq}}} \approx \frac{1}{R_{\theta,\text{int}}} + \frac{1}{R_{hl}} + \frac{1}{R_g}. \tag{3}$$

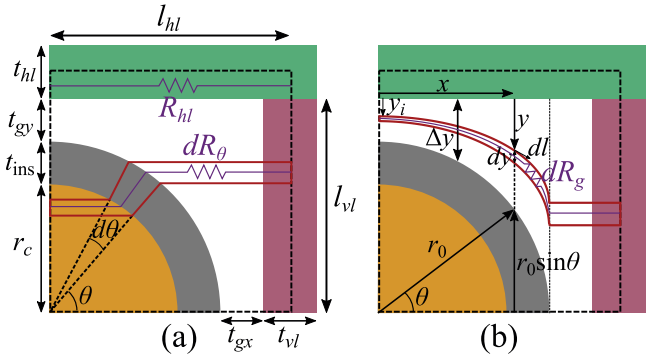

Fig. 4. A quarter-unit cell (black dashed box) of square-packed wires showing various thermal resistances. Thermal resistance is calculated for unidirectional heat flow from left to right. The red enclosed areas show path of integration for the infinitesimal thermal resistances (a) dR_θ given by (5) and (b) dR_g given by (12).

As discussed above, the parallel combination is only approximate based on the asymptotic behavior of the effective thermal resistance for very high and very low k_g; it may underestimate R_{sq} for intermediate values of k_g.

$R_{\theta,\text{int}}$ can be calculated as a parallel combination of thermal resistance for infinitesimal θ represented by the red enclosed area and dR_θ in Fig. 4 (a):

$$\frac{1}{R_{\theta,\text{int}}} = \int_{\theta=0}^{\frac{\pi}{2}} \frac{1}{dR_\theta}, \tag{4}$$

$$dR_\theta = dR_{\theta,c} + dR_{\theta,\text{ins}} + dR_{\theta,g} + dR_{\theta,vl}, \tag{5}$$

$$dR_{\theta,c} = \frac{r_c \cos\theta}{k_c \; r_c \cos\theta \; d\theta \; l_l} = \frac{1}{k_c \; d\theta \; l_l}, \tag{6}$$

$$dR_{\theta,\text{ins}} = \frac{\ln(r_0/r_c)}{k_{\text{ins}} \; d\theta \; l_l}, \tag{7}$$

$$dR_{\theta,g} = \frac{r_0(1-\cos\theta) + t_{gx}}{k_g \; r_0 \cos\theta \; d\theta \; l_l}, \text{ and} \tag{8}$$

$$dR_{\theta,vl} = \frac{t_{vl}/2}{k_{vl} \; r_0 \cos\theta \; d\theta \; l_l}, \tag{9}$$

where l_l is the wire length, and $r_0 = r_c + t_{\text{ins}}$ the total wire radius (Fig. 4 (b)).

R_{hl} is the thermal resistance across the green horizontal layer (Fig. 4 (a)) and is given by

$$R_{hl} = \frac{l_{hl}}{k_{hl} \; (t_{hl}/2) \; l_l} = \frac{2 l_{hl}}{k_{hl} \; t_{hl} \; l_l}. \tag{10}$$

R_g is the thermal resistance across the gap, represented by the white region in Fig. 4. It is defined specifically for heat flowing through the gap above the wire insulation and spreading out inside the gap (purple arrow labeled 2b in Fig. 3 (a)) and is given by

$$\frac{1}{R_g} = \int_{y_i=0}^{t_{gy}} \frac{1}{dR_g}, \tag{11}$$

where dR_g is the infinitesimal thermal resistance, represented by the red enclosed area in Fig. 4 (b).

It is assumed that heat spreads out from left to right proportional to the total width of the gap Δy at any horizontal position x. In other words, heat at a vertical position y_i at the left end of the quarter-unit cell flows towards a vertical position $y = y_i \Delta y(x)/\Delta y(0)$ at a horizontal position x,

and heat spreads out from an infinitesimal width dy_i to $dy = dy_i \Delta y(x)/\Delta y(0)$. It can be derived that

$$dR_g = \frac{1}{k_g l_l dy_i}\left(\frac{t_{gx} t_{gy}}{r_0 + t_{gy}} + \int_0^{\frac{\pi}{2}} \frac{d\theta\ r_0 \sqrt{t_{gy}^2 \sin^2\theta + y_i^2 \cos^2\theta}}{r_0 + t_{gy} - r_0 \sin\theta}\right), \tag{12}$$

where y_i refers to the vertical position y at $x = 0$, dy_i the infinitesimal y_i, dR_g the infinitesimal thermal resistance across the red enclosed area in Fig. 4 (b), and t_{gx} and t_{gy} are defined in Fig. 4 (b). The detailed derivation of (12) is discussed in [8].

Heat flow inside the gap is modeled using two thermal resistances: $R_{\theta,g}$ and R_g. The former, $R_{\theta,g}$, models the resistance for heat flowing across the wire and continuing into the gap, represented by the portion of the red enclosed area in the gap in Fig. 4 (a). The latter, R_g, models the gap thermal resistance for heat flowing through the gap above the wire and spreading out in the gap, represented by the red enclosed area in Fig. 4 (b). Because of the intersection between the cross-sectional area modeled by these two variables, there is some effect of double counting which can result in underestimating R_{sq}; however, both $R_{\theta,g}$ and R_g are necessary. First, for low k_g, most of the heat will flow across the wire rather than the gap above the wire, and $R_{\theta,g}$ is necessary in order not to underestimate $R_{\theta,\text{int}}$ and R_{sq}. On the other hand, for large k_g, most of the heat will flow across the gap above the wire, in which case R_g is necessary in order not to overestimate R_{sq}. The effect of double counting is the most significant when $R_{\theta,\text{int}}$ and R_g are on the same order of magnitude; however, the error due to this double counting is less than 15%, as will be discussed in Section IV-A.

D. Transverse Thermal Resistance: Hexagonal-Packed Wires

The thermal resistance of a unit cell of hexagonal-packed wires, shown in Fig. 5 (a), is a parallel combination of thermal resistance for heat flow between the centers of two adjacent conductors $R_{\theta,\text{int}}$ (red arrow labeled 2a in Fig. 3 (b), integral of dR_θ in Fig. 5 (a) with respect to θ) and gap thermal resistance R_g (purple arrow labeled 2b in Fig. 3 (b), integral of dR_g in Fig. 5 (b) with respect to r_i):

$$\frac{1}{R_{\text{hex}}} \approx \frac{1}{R_{\theta,\text{int}}} + \frac{1}{R_g}. \tag{13}$$

It should be noted that the parallel combination is only an approximation, as discussed above.

$R_{\theta,\text{int}}$ is a parallel combination of infinitesimal thermal resistance at different values of θ:

$$\frac{1}{R_{\theta,\text{int}}} = 4\int_{\theta=0}^{\frac{\pi}{3}} \frac{1}{dR_\theta}, \tag{14}$$

$$dR_\theta = dR_{\theta,c1} + dR_{\theta,\text{ins1}} + dR_{\theta,g} + dR_{\theta,\text{ins2}} + dR_{\theta,c2}, \tag{15}$$

where the subscript 1 refers to the first wire, marked by $d\theta$ in Fig. 5 (a) and the subscript 2 the second wire, marked by $d\varphi$. The integral in (14) is multiplied by 4 since the integration gives the thermal resistance of a quarter of the unit cell, represented by the green shaded area in Fig. 5 (a), and a unit cell contains four such areas in parallel. It should be noted that as the gap gets larger, φ gets smaller and the portion of the second wire covered by the green shaded area in Fig. 5 (a) gets relatively small. Because the entirety of the second wire is not accounted for in $R_{\theta,g}$, this model can overestimate $R_{\theta,\text{int}}$ and hence R_{hex}.

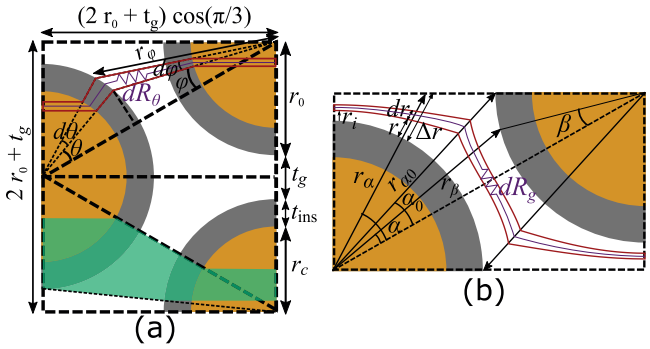

Fig. 5. Hexagonal-packed wires showing various thermal resistances. Thermal resistance is calculated for unidirectional heat flow from left to right. (a) A unit cell showing the infinitesimal thermal resistance dR_θ given by (15) and (b) a half-unit cell showing the infinitesimal thermal resistance dR_g given by (25). The red enclosed areas show paths of integration.

The resistances $dR_{\theta,c1}$ and $dR_{\theta,c2}$ represent the conductors of the two wires and are similar to (6):

$$dR_{\theta,c1} = \frac{1}{k_c\ d\theta\ l_l}, \tag{16}$$

$$dR_{\theta,c2} = \frac{1}{k_c\ d\varphi\ l_l}. \tag{17}$$

For each value of θ for the first wire, a corresponding angle φ can be defined for the second wire as shown in Fig. 5 (a); as θ increases from 0 to $\pi/3$, φ increases from 0 to around $\pi/6$ depending on the gap width. The infinitesimal angle $d\varphi$ can be written in terms of $d\theta$ as

$$d\varphi = \frac{2r_0^2 \cos\theta + r_0 t_g \cos\theta - r_0^2}{r_\varphi^2} d\theta, \tag{18}$$

$$r_\varphi = \sqrt{r_0^2(5 - 4\cos\theta) + 2r_0 t_g(2 - \cos\theta) + t_g^2} \tag{19}$$

where r_φ is the distance from the center of the second wire to the edge of the first wire at the angle θ, as shown in Fig. 5 (a). The derivation of $d\varphi$ and r_φ is discussed in [8].

The resistances $dR_{\theta,\text{ins1}}$ and $dR_{\theta,\text{ins2}}$ are represent the insulation of the two wires and are similar to (7):

$$dR_{\theta,\text{ins1}} = \frac{\ln(r_0/r_c)}{k_{\text{ins}}\ d\theta\ l_l}, \tag{20}$$

$$dR_{\theta,\text{ins2}} = \frac{\ln(r_0/r_c)}{k_{\text{ins}}\ d\varphi\ l_l}. \tag{21}$$

The resistance $dR_{\theta,g}$ models the thermal resistance of the gap for heat flowing between the centers of two adjacent wires (red enclosed area in Fig. 5 (a)), and is given by

$$dR_{\theta,g} = \frac{\ln(r_\varphi/r_0)}{k_g\ d\varphi\ l_l}. \tag{22}$$

This is distinct from R_g in (13) which models the gap thermal resistance for heat coming in from the left through the gap above the wire (red enclosed area in Fig. 5 (b)).

Calculation of the gap thermal resistance R_g is similar to that for square packing; it is assumed that heat spreads out proportional to the radial width of the gap Δr at an arbitrary

angular position α; the radial position $r = r_i \Delta r(\alpha)/\Delta r(\pi/3)$ and infinitesimal radial width $dr = dr_i \Delta r(\alpha)/\Delta r(\pi/3)$, where r_i and dr_i are the radial position and infinitesimal radial width at $\alpha = \pi/3$. The specific path of integration is shown in red enclosed area in Fig. 5 (b). The gap thermal resistance R_g can be written as

$$\frac{1}{R_g} = 2\int_{r_i=0}^{\frac{t_g}{2}} \frac{1}{dR_g}. \tag{23}$$

$$dR_g = \frac{1}{k_g l_l}\left(\int_{\beta=0}^{\frac{\pi}{6}}\left(\frac{dl}{dr}+\frac{dl'}{dr'}\right)+\int_{\alpha=\alpha_0}^{\frac{\pi}{3}}\left(\frac{dl}{dr}+\frac{dl'}{dr'}\right)\right) \tag{24}$$

$$= \frac{1}{k_g l_l}\int_{\beta=0}^{\frac{\pi}{6}}\left(\frac{r_0 + r_i\frac{r_\beta - r_0}{t_g/2}}{dr_i\frac{r_\beta - r_0}{t_g/2}} + \frac{r_\beta - r_i\frac{r_\beta - r_0}{t_g/2}}{dr_i\frac{r_\beta - r_0}{t_g/2}}\right) \frac{2r_0^2\cos\beta + r_0 t_g\cos\beta - r_0^2}{r_\beta^2}\, d\beta \tag{25}$$

$$+ \frac{1}{k_g l_l}\int_{\alpha=\alpha_0}^{\frac{\pi}{3}}\left(\frac{r_0 + r_i\frac{r_\alpha - r_0}{t_g/2}}{dr_i\frac{r_\alpha - r_0}{t_g/2}} + \frac{r_\alpha - r_i\frac{r_\alpha - r_0}{t_g/2}}{dr_i\frac{r_\alpha - r_0}{t_g/2}}\right) d\alpha,$$

$$r_\beta = \sqrt{r_0^2(5-4\cos\beta) + 2r_0 t_g(2-\cos\beta) + t_g^2}, \tag{26}$$

$$r_\alpha = \left(r_0 + \frac{t_g}{2}\right)\sec\left(\frac{\pi}{3} - \alpha\right) \tag{27}$$

$$\alpha_0 = \arctan\frac{r_0}{(4-\sqrt{3})r_0 + 2t_g}, \tag{28}$$

Derivation of (25) is similar to that of (12) and is discussed in [8]. The integration with respect to r_i gives the thermal resistance of half a unit cell, thus requiring the factor of 2 multiplying the integral in (23).

E. Thermal Resistance of a Group of Wires

The proposed model gives the effective thermal resistance of a unit cell inside a group of wires. Thus, the result from the proposed model needs to be scaled with respect to the number of wires in order to calculate the effective resistance of the entire group of wires R_{eff}. The effective longitudinal thermal resistance a group of wires is given by

$$R_{\text{eff},l} = \frac{R_l}{N}, \tag{29}$$

where R_l is the longitudinal resistance of a unit cell given by (1) and N is the number of wires. For the transverse direction, the effective thermal resistance is

$$R_{\text{eff},t} = \frac{N_x}{N_y} R_t, \tag{30}$$

where R_t is the unit-cell transverse thermal resistance of the packing of choice (R_{sq} or R_{hex}), and N_x and N_y are respectively the number of wires along and perpendicular to the direction for which the thermal resistance needs to be calculated. For instance, for heat flow from left to right in Fig. 3 (a), N_x is the number of wires in the horizontal direction from left to right (i.e. 3) and N_y is the number of wires in the vertical direction from top to bottom (i.e. 3).

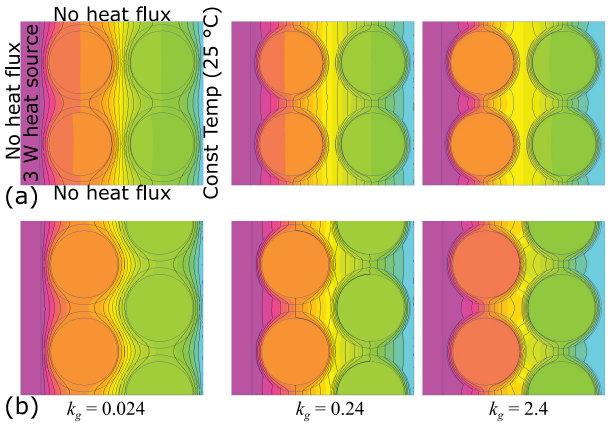

Fig. 6. Sample finite element simulations for (a) square packing and (b) hexagonal packing; results for three different values of gap thermal conductivity k_g are included. The black curves are isothermal and the blue curves represent boundaries between different materials. The boundary conditions are defined to obtain heat flow from left to right. A known heat source (3 W) is placed to the left of the group of wires; the heat source is in a high thermal-conductivity material in order to provide an isothermal boundary. The known heat source and the temperature difference between the two ends of the group of wires is used to calculate thermal resistance.

If effective thermal conductivity k_{eff} rather than effective thermal resistance R_{eff} is desired, the unit cell thermal resistances can be scaled by the length of wire l_l used in the winding. The effective transverse thermal conductivity is

$$k_{\text{eff},t} = \frac{N_x}{N_y\ l_l\ R_{\text{eff},t}} = \frac{1}{R_t l_l}. \tag{31}$$

The effective longitudinal thermal conductivity is given by (2).

IV. Accuracy Assessment Using Finite Element Analysis

Finite element analysis (FEA) was used to test the accuracy of the proposed model for square and hexagonal packings. Fig. 6 shows the results of sample simulation results with 4 strands of wire ($N_x = N_y = 2$) for square and hexagonal packing. It is a 2D simulation which represents the cross-section of wires, and does not account for twisting of the wires along the length. It should be noted that Fig. 6 (b) is not equivalent to 4 unit cells of hexagonal-packed wires, as defined in Figs. 3 (b) and 5 (a). The wires are arranged to obtain a rectangular outer shape. A known heat source is placed to the left of the wires and a constant temperature boundary condition to the right of the wires. The other boundaries are defined with no heat flux conditions to obtain a unidirectional heat flow from left to right. The temperature at the heat source is extracted to calculate the thermal resistance across the group of wires.

Fig. 6 shows the result of FEA, using FEMM, for three different gap thermal conductivity k_g: 0.024 representing air, 0.24 representing many plastic materials and 2.4 representing thermally conductive epoxy resin potting. The simulations were conducted for wires with 1 mm copper diameter, 0.1 mm insulation thickness and 0.1 mm separation between wires; the thermal conductivities of the wire and the wire insulation coating are respectively 385 $\text{W}/(\text{m}\cdot\text{K})$ (representing copper) and 0.028 $\text{W}/(\text{m}\cdot\text{K})$ (modified polyurethane). The particular

TABLE II
VALUES OF t_{ins}, t_g AND k_g USED FOR ACCURACY ASSESSMENT.

t_{ins}	t_g	k_g W/(m · K)	Representing material
d_c/50	$(d_c + 2t_{\text{ins}})$/50	0.024	air
d_c/20	$(d_c + 2t_{\text{ins}})$/20	0.2	most plastic
d_c/10	$(d_c + 2t_{\text{ins}})$/10	1	-
d_c/5	$(d_c + 2t_{\text{ins}})$/5	4	epoxy resin potting
	$(d_c + 2t_{\text{ins}})$/2	20	-

Note: Each row does not correspond to a combination of t_{ins}, t_g and k_g. 100 different combinations can be formed using the values in the table.

dimensions in Fig. 6 were chosen to show the salient features; the insulation thickness and the gap in practical windings will be much smaller. Fig. 6 shows that the heat paths for low and high values of the gap thermal conductivity are qualitatively different; for low k_g, heat flow is concentrated near the region where the wires are spatially closest in the horizontal direction whereas heat mainly flows through the gap between wires for high k_g.

The FEA was performed for various combinations of parameters. Because the unit-cell thermal resistance is independent of the number of wires (N, N_x or N_y), we used $N = 1$ to simulate a unit cell, as defined in Fig. 3. Moreover, the thermal resistance does not depend on the absolute value of the wire diameter d_c, but on the relative value of d_c with respect to the insulation thickness t_{ins} and gap between wire t_g, defined for square packing as $t_g = 2t_{gx} = 2t_{gy}$. Thus, we used $d_c = 127$ µm (AWG 36) and vary t_{ins} and t_g relative to d_c. Four different values were considered for t_{ins}, five for t_g and five for k_g, as described in Table II. For each of these 100 combinations of t_{ins}, t_g and k_g, the result from the proposed model is compared to that from FEA. It is assumed that there are no horizontal or vertical insulation layers.

A. Proposed Model

Fig. 7 shows the errors of the proposed model compared to FEA for both square and hexagonal packing, calculated as

$$\text{Error } (\%) = \frac{R_{\text{eff},t,\text{model}} - R_{\text{eff},t,\text{FEA}}}{R_{\text{eff},t,\text{FEA}}} \times 100\%, \qquad (32)$$

where $R_{\text{eff},t,\text{model}}$ and $R_{\text{eff},t,\text{FEA}}$ are effective transverse thermal resistances predicted by the model and FEA, respectively.

For square packing (Fig. 7 (a)), the error for $k_g = 0.024$ W/(m · K), representing air, is less than 6%; it is larger for higher k_g but less than 15% for the entire range of k_g and for all the combinations of t_{ins} and t_g considered. It should be noted that most of these errors are negative, indicating that the proposed model underestimates the thermal resistance. This underestimation error can be attributed to the double counting of gap thermal resistance as discussed in Section III-C. Because of this double counting, the proposed model is less accurate for moderate values of k_g; nevertheless, the error is below 15% even with the effect of double counting.

The results for hexagonal-packed wires for the two models are shown in Fig. 7 (b). The proposed model has a maximum error of 18.5% for all the cases considered, and the error for higher k_g is lower than that for lower k_g. Unlike square packing, however, most of the errors are positive, indicating

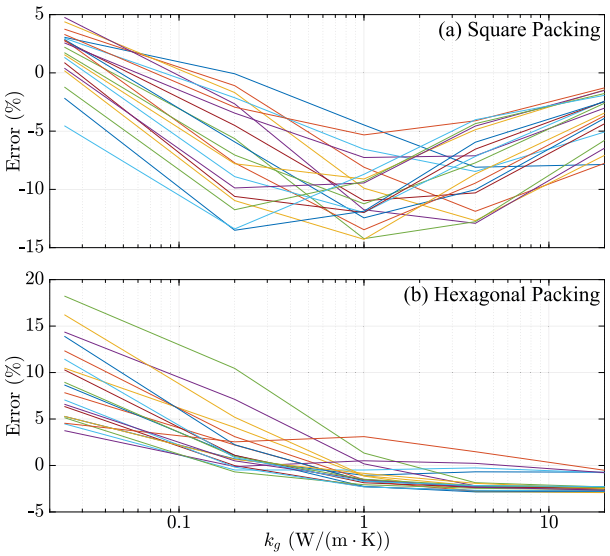

Fig. 7. Percentage error of the proposed model compared to FEA for (a) square-packed and (b) hexagonal-packed wires. Each curve corresponds to a particular combination of t_{ins} and t_g.

that the proposed model overestimates the thermal resistance. This overestimation can be attributed to the fact that $R_{\theta,\text{int}}$ only cover the green shaded area of each quarter of the unit cell in Fig. 5 (a). The overestimation is more significant for lower k_g since more heat will flow through the wire rather than the gap above the wire, and for larger t_g since the green shaded area in Fig. 5 (a) is smaller. Unlike the square packing case, the negative errors for the hexagonal packing case are relatively small; this may be attributed to the overestimation error discussed above partially canceling the underestimation error due to double counting.

B. TEFA Model

For comparison, the errors of the TEFA model compared to the results of the FEA were also calculated using (32), which are plotted in Fig. 8. It should be noticed that the FEA is a 2D simulation, conducted for cross-sections of wires as shown in Fig. 6; it does not model any twisting or change in position of wire along the length of the wire. From Fig. 8, it can be seen that the TEFA model cannot accurately predict the effective thermal resistance for both square and hexagonal packing for large values of gap thermal conductivity k_g. Thus, the proposed model can provide better prediction for the effective thermal resistance of a group of insulated round wires.

It should be noted that the errors in Fig. 8 were calculated using the TEFA model as presented in [6], which assumes that the wires are touching one another with the exception of a vertical insulation layer. Thus, the errors are large if heat flow is significantly impacted by the gap, such as in cases with a large separation between wires t_g and or with a high gap thermal conductivity k_g. Modifications to the TEFA model, such as using the vertical insulation layer to account for the gap in the horizontal direction, can reduce the error of the TEFA model. The proposed model provides such modification considering how the heat spread out inside the gap.

Moreover, the errors in Figs. 7 and 8 are plotted for a wide range of parameters as described in Table II. The range of

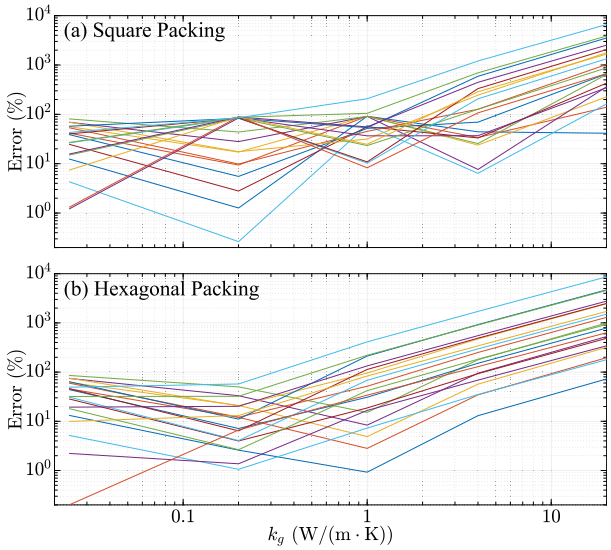

Fig. 8. Absolute value of the percentage error of the TEFA model compared to FEMM simulation for (a) square-packed and (b) hexagonal-packed wires. Each curve corresponds to a particular combination of $t_{\rm ins}$ and t_g. The errors are plotted on the logarithmic scale. Points with very large errors correspond to cases with high gap thermal conductivity k_g and or large gaps (large values of t_g, t_{gx}, t_{gy}).

parameters for practical windings are more limited, which will result in smaller errors. For example, k_g up to 20 $\mathrm{W/(m \cdot K)}$ are considered in Figs. 7 and 8 whereas windings potted with epoxy resin have $k_g \lesssim 4$ $\mathrm{W/(m \cdot K)}$. Similarly, practical ranges of wire insulation thickness $t_{\rm ins}$ and separation between wires t_g will further narrow the range of errors in Fig. 8. Nevertheless, the proposed model can provide a smaller error compared to the TEFA model for a wider range of parameters or cases. For instance, the proposed model is useful for litz wire which usually has a low packing factor and for potted windings which have a high gap thermal conductivity.

V. Practical Application of the Proposed Model

The proposed analytical model calculates the thermal resistance of a group of wires regularly arranged in square or hexagonal packing. The model only requires knowledge of various parameters, such as geometric dimensions and thermal conductivities of the constituent materials. Finite element analysis (Section IV) shows that the analytical model is accurate, with an error of less than 20% for a wide range of parameters. However, practical inductor and transformer windings and litz wire usually have random packing and some parameters may not be readily available. This section discusses implementation of the model and how it can be used to calculate effective thermal resistance or conductivity of practical inductor and transformer windings and litz wire, as well as various limitations of the model.

A. Implementation

The proposed model can be implemented using (3)–(28). For square packing, $R_{\rm sq}$ is a parallel combination of $R_{\theta,\rm int}$, R_{hl} and R_g as shown in (3). $R_{\theta,\rm int}$ can be calculated by integration (4) of a combination (5) of four infinitesimal thermal resistances (6)–(9). R_{hl} is a simple calculation (10) and R_g can be found by integrating (11) the infinitesimal resistance given by (12). For hexagonal packing, $R_{\rm hex}$ is a parallel combination of $R_{\theta,\rm int}$ and R_g as shown in (13). $R_{\theta,\rm int}$ can be found by integrating (14) a combination (15) of five infinitesimal thermal resistances (16), (17) and (20)–(22). R_g is found by integrating (23) the infinitesimal resistance given by (25). Implementing the model for hexagonal packing also requires (18), (19) and (26)–(28).

B. Random Packing

The packing of strands inside a litz-wire bundle and of wires in an inductor or transformer winding is usually random, and so neither square nor hexagonal packing can accurately describe the effective thermal resistance of practical windings and litz wire. However, a random packing can be considered as some combination of local square and hexagonal packing. Thus, the effective thermal resistance of practical windings and litz wire can be approximated as a weighted average of thermal resistances for square and hexagonal packings.

The appropriate weight depends on the particular types of winding. For windings in which an insulation tape separates different layers, no weight needs to be given for hexagonal packing; the square packing model alone is sufficient. For windings without an insulation tape between layers, a relatively higher weight should be assigned for the hexagonal packing model. For windings with a large number of turns or litz wire with many fine strands, a simple average with equal weight between the two packings (i.e. arithmetic mean) can be sufficient since the packing becomes more random as the number of turns or strands increases. It should be noted that the arithmetic mean is a simple heuristic for modeling random packing; different types of average, such as the geometric mean, do not have a significant impact on the result as will be discussed in Section VI-D. During the design stage of magnetics when the packing of wire is not known, the arithmetic mean can also be used as a simple rule of thumb to approximately calculate the effective thermal resistance or conductivity. Experimental verification of the results of the proposed model for a practical inductor with random packed litz wire is discussed in Section VI.

C. Litz Wire

Typical specifications for litz wire include the number of strands N, the strand gauge or diameter d_c and the overall diameter of the bundle $d_{\rm tot}$. The thickness of enamel insulation coating $t_{\rm ins}$ can be found by consulting the wire standard (e.g., NEMA MW 1000 [9]) or using a curve-fit formula of data from a wire manufacturer's catalog, such as that in [10]. The thermal conductivity of enamel is usually around 0.03 $\mathrm{W/(m \cdot K)}$ [11]. The gap between wire strands, which is typically not specified, can be calculated from the known parameters. For square packing, $t_g = 2t_{gx} = 2t_{gy}$ can be calculated by equating the overall area of the bundle $A_{\rm tot} = \pi d_{\rm tot}^2/4$ to the total area of N unit cells $N(d_c + 2t_{\rm ins} + t_{gx})(d_c + 2t_{\rm ins} + t_{gy})$. For hexagonal packing, $A_{\rm tot}$ is equated to $N(d_c + 2t_{\rm ins} + t_g)^2 \cos(\pi/6)$.

For the scaling of the unit cell thermal resistance with respect to the number of wires as given by (30), N_x and N_y usually cannot be accurately estimated. However, because litz wire usually comprises a large number of strands, the ratio N_x/N_y can be approximated as the ratio of linear dimensions along and perpendicular to the direction for which the thermal resistance needs to be calculated. For example, for litz wire with a square outer shape, the overall transverse thermal resistance $R_{\mathrm{eff},t}$ equals the unit cell effective resistance R_t.

Twisting of wire strands in litz wire can impact the transverse thermal resistance because a wire strand at one side of the bundle will eventually arrive at the other side of the bundle at some point along the length of the litz wire depending on the pitch of twisting. However, such effect is negligible because thermal resistance along a single strand is large compared to that across the diameter, especially for twisting pitch much longer than the bundle diameter. For litz wire with a short twisting pitch, the proposed model can be combined with the effect of twisting presented in [6] to more accurately model the litz-wire transverse thermal resistance.

Depending on the application, the litz-wire bundle may be enclosed in an outer insulation layer. In such cases with two levels of insulation, the effective thermal conductivity k_{eff} of wire strands, without the outer insulation layer, can be calculated using the proposed model. This k_{eff} can then be used as k_c and the outer insulation layer thickness as t_{ins} in a second iteration of the proposed model to calculate the overall thermal resistance and effective conductivity.

D. Inductor and Transformer Windings

Inductor and transformer windings can be made of either solid wire or litz wire. For solid wire windings, with one level of insulation, the proposed model can simply be used to calculate the unit cell thermal resistance. The gap between wires, or turns, can be calculated by equating the overall winding area to the total area of N turns of wires. For litz-wire windings, with two levels of insulation, the effective thermal conductivity of litz wire needs to be calculated as discussed in Section V-C, which can then be used to calculate the overall thermal resistance.

E. Parameter Values

Knowledge of material properties and geometric dimensions of winding and litz wire is necessary for accurate modeling. Some of these parameters can change during the winding process. For example, litz-wire bundle diameter d_{tot} inside a winding may be different from the nominal diameter provided in the specifications. In such cases, the nominal diameter should be corrected with an estimated winding factor. Some parameters are difficult to estimate. For instance, in practical inductors and transformers with potted windings, although the potting resin can seep through the wires, it may not entirely fill the gaps between the wires depending on the gap width and the potting viscosity. In such cases, the gap thermal conductivity can be approximated as an average of the thermal conductivities of air and potting resin, weighted by the degree of potting fill. The difficulty and uncertainty in estimating the degree of potting fill can lead to errors in calculating the effective thermal resistance using the proposed model.

It should be noted that these challenges regarding parameter values are not specific to the proposed model; models, in general, have to use nominal or estimated parameter values since the actual values are usually not known during the design process or are hard to measure.

F. Application in a Thermal Network Model

The proposed model provides discrete thermal resistance across a unit cell, which is then scaled to obtain the winding thermal resistance along a particular direction. However, heat is often generated uniformly inside inductor and transformer windings, so the discrete thermal resistance of the proposed model may overestimate the overall thermal resistance from one side of the winding to the other. The generated heat also spreads in three dimensions rather than the unidirectional heat flow assumed in the proposed model. Thus, accurate modeling of the entirety of an inductor or a transformer requires calculating the anisotropic thermal resistance along three orthogonal directions. These thermal resistances are then to be used as a component in a thermal network model, as discussed in Section II, in which the effective thermal resistance from the proposed model is a component among other. The effective thermal conductivity can also be used as part of finite element analysis which models the winding area as a single material omitting the detailed strand structures. The application of the analytical thermal model of litz wire in a thermal network model for a practical inductor is discussed in the following section.

VI. Experimental Verification

The analytical thermal model in Section III provides a way to calculate the effective thermal resistance and conductivity of a group of wires regularly arranged in a square or hexagonal packing, and the accuracy of the model was verified using finite element analysis as discussed in Section IV. This section discusses experimental verification of the proposed model in practical inductor windings, with random-packed wires.

A preliminary check of the proposed model was performed by applying the proposed model to the litz wire samples $TS_{L,air,1}$ and $TS_{L,air,2}$ in Table II of [6]. For the $TS_{L,air,2}$ sample with measured effective thermal resistance $R_{w,x} = 2.1$ K/W, the proposed model gives $R_{w,x} = 2.38$ K/W (13.33% error). This error is larger than the -0.5% error of the TEFA model with twisting, but smaller than the 38.57% error of the TEFA model without twisting. It should, however, be noted that the higher error of the proposed model compared to the TEFA model with twisting can partly be attributed to inexact knowledge of the geometrical parameters provided in [6]. For example, the proposed model cannot be applied to the $TS_{L,air,1}$ sample since the tabulated characteristics of the sample result in a packing factor of 0.924, which is higher than the theoretical maximum packing factor. In other words, these samples are compressed to fit into a tight space, causing the wire radii in the experimental setup to be smaller than the nominal radii. Better knowledge of these litz wire samples as

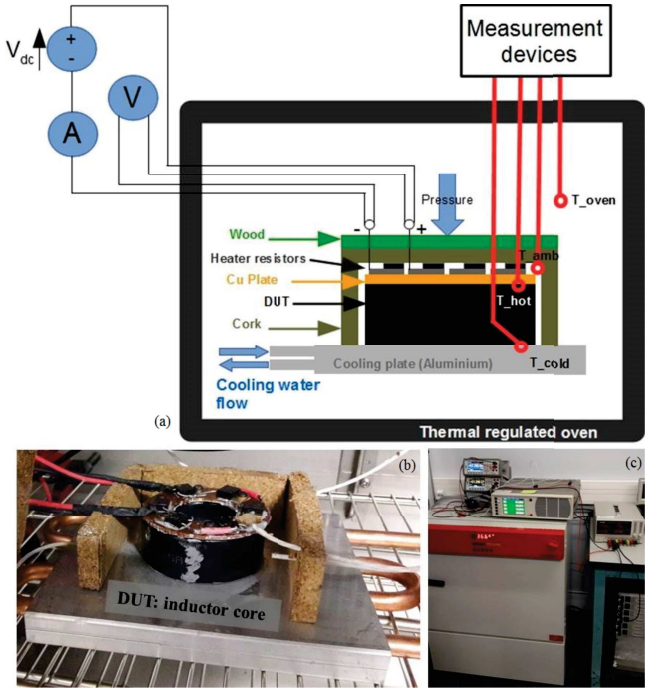

Fig. 9. Experimental test setup. (a) Test bench schematic, (b) test bench picture, and (c) instrumentations.

they are in the experimental setup of [6] is required for a fair comparison of the proposed model and the TEFA model.

The experimental verification for this paper was conducted using the toroidal inductor in Fig. 1. An optimization algorithm [7] was used to obtain the effective thermal conductivity of litz wire in the inductor from experimental temperature measurement and the thermal network model of the toroidal inductor.

A. Experimental Set Up

The thermal resistance of the toroidal inductor was measured using the thermal test bench shown in Fig. 9. The inductor, or device under test (DUT), was placed on a cooling base plate with a set temperature. Heater resistors placed on a copper plate on top of the DUT generate a fixed amount of heat, hence a temperature gradient across the DUT. The measured temperature gradient ΔT and the generated heat Q can be used to calculate the thermal resistance across the DUT:

$$R_{DUT} = \frac{\Delta T}{Q}. \tag{33}$$

Another thermocouple was placed between the magnetic core and litz wire at the bottom of the DUT (Fig. 10) for direct measurement of thermal resistance between the hot plate and the bottom of the core R_1 and that between the bottom of the core and the cooling plate R_2.

Accurate determination of the thermal conductivity of different constituent materials requires negligible convection and radiation from the DUT, and good thermal contact from the DUT to the heater resistors and the cooling plate. Thus, the DUT was placed inside a closed cork box with $k_{\text{cork}} = 0.04\ \text{W}/(\text{m}\cdot\text{K})$ in a oven with regulated temperature. The oven temperature is regulated at the mean value of cold plate and hot plate temperatures to limit convection. Thermal paste ($k_{\text{paste}} = 10\ \text{W}/(\text{m}\cdot\text{K})$) [12] with a supposed thickness of 500 µm is applied to the DUT and a pressure of 78 N is applied through a wooden plate to ensure a good thermal contact between the DUT and the heating and the cooling plates.

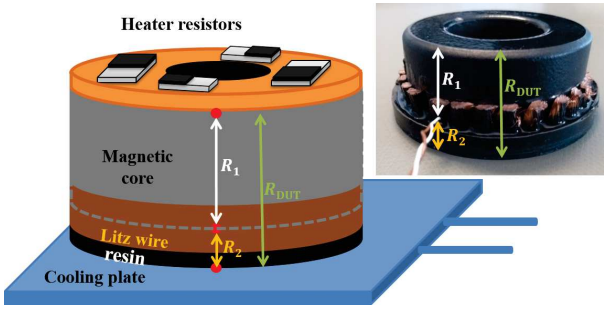

Fig. 10. Schematic of the samples showing measurements for thermal resistances R_1, R_2 and R_{DUT}.

TABLE III
LITZ-WIRE SAMPLES

Litz sample	#1	#2	#3	#4
Number of strands	81	320	210	855
Strand diameter (mm)	0.2	0.1	0.2	0.1
Strand insulator thickness (µm)	12.5	8	12.5	8
Number of bundles	9	10	10	5
Strand pitch length (mm)	11.8	18.9	29.3	23.3
Measured external diameter (mm)	2.56	2.74	4.92	5

A brass sample with a known thermal conductivity was used to validate the thermal test bench. This sample has the same internal and external diameters as the sample toroidal inductor, but is 3.44 times thicker to obtain a measurable gradient of temperatures along this sample with relatively high conductivity. A high-conductivity material was chosen for this validation setup in order to determine the upper bound for measurement uncertainty; the same uncertainty in temperature measurement will result in a much lower error for estimating the thermal conductivity of litz wire, which is typically about two orders of magnitude smaller than that of brass. The error between the measured and the estimated thermal resistance of this brass sample is 10.7%, attributable to measurement uncertainty, ignored convection and impurities in the sample. The measurement on the sample is also reproducible, with only 0.5% difference in results between different measurements.

B. Samples and Measurement Results

In order to ensure that the analytical model (Section III) is applicable for a variety of cases, the thermal measurement is performed on various samples of litz wire and inductor.

1) Litz-Wire Samples: Four different samples of litz wire, described in Table III, were used. Two of the litz samples (#1 and #2) have similar copper section as well as the other two litz samples (#3 and #4). Two samples (#1 and #3) have the same strand diameter to address the same switching frequency, and so do the other two samples (#2 and #4).

2) Inductor Samples: The molding of the inductor and the number of turns in the winding were also varied. In order

TABLE IV
MEASUREMENT RESULTS OF THE DIFFERENT SAMPLES. FOR SAMPLE 4, R_1 AND R_2 ARE EXCLUDED BECAUSE OF A FAILED THERMOCOUPLE.

Sample	1	2	3	4	5	6	7
Litz	#1	#2	#3	#4	#4	#4	#4
Molding height	Bottom	Bottom	Top	Bottom	Top	Bottom	Top
Layer fill rate	100%	100%	100%	100%	100%	66%	66%
R_1 (K/W)	3.17	3.04	2.15	-	1.71	3.10	1.72
R_2 (K/W)	0.82	0.76	0.92	-	0.57	0.74	0.76
R_{DUT} (K/W)	4.00	3.80	3.07	3.50	2.28	3.85	2.49

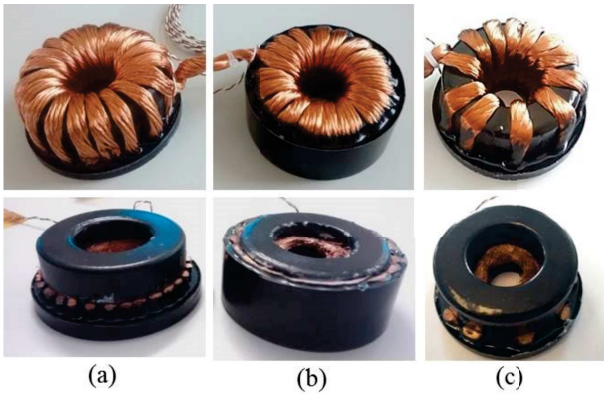

Fig. 11. Sample pictures. Top: before the litz wire cutting, bottom: after the litz wire cutting (used for measurements). (a) molded only at the bottom and 100% layer fill rate, (b) molded to the top and 100% layer fill rate, (c) molded only at the bottom and 66% layer fill rate.

to test the impact of the litz wire on the side, four inductor samples (1, 2, 4 and 6) were molded only at the bottom of the inductor as shown in Fig. 11 (a) whereas three samples (3, 5 and 7) were molded up to the top of the inductor (Fig. 11 (b). Samples 1, 2, 4 and 6, in which the inductor is molded only at the bottom, effectively provides a setup for direct measurement of the litz wire transverse thermal conductivity whereas the other samples are also influenced by the longitudinal thermal conductivity. All the samples have a single-layer winding but some samples (6 and 7) have fewer turns such that the winding covers only 66% of the core in order to check the impact of layer fill rate. Fig. 11 (c) shows an inductor with partial winding filling which is molded only at the bottom. The impact of the number of strands within a litz wire is also analyzed on the samples. These different samples are summarized in Table IV.

3) Measurement Results: The thermal resistances R_1 (from the hot plate to the bottom of the core), R_2 (from the bottom of the core to the cooling plate) and R_{DUT} ($R_1 + R_2$) as shown in Fig. 10 were calculated from the known generated heat and the measured temperature gradient, and the results are summarized in Table IV. These results can be used to obtain the effective thermal resistances of litz wire since the thermal properties of all other materials (epoxy, resin, core) as well as the contact thermal resistances (thermal paste) are known. Comparison of R_{DUT} of samples 4 and 5 to that of samples 6 and 7 shows that higher layer fill rate reduces the thermal resistance of the DUT. Thus, litz wire along the side of the core improves thermal conduction compared to the molding resin.

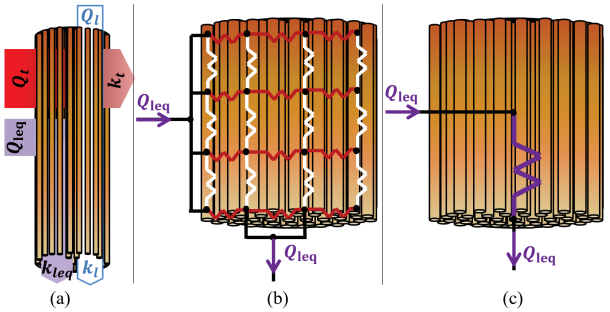

Fig. 12. Definition of litz-wire thermal conductivities. (a) Path of different heat sources, (b) transverse and longitudinal resistances, as a thermal network inside the litz wire, (c) definition of the longitudinal equivalent thermal resistance with conductivity k_{leq} substituting the thermal network in (b).

C. Identification of Litz-Wire Conductivities

The effective thermal conductivities of litz-wire samples were determined using an optimization strategy based on the experimental data. Because of the anisotropic behavior of litz wire, two effective thermal conductivities need to be determined, namely transverse (k_t) and longitudinal (k_l) as shown in Fig. 12. A thermal network model, similar to the 2D model in Fig. 2, was developed for each sample and the unknown parameters (k_t and k_l) were adjusted by the optimization algorithm to minimize the difference between the temperatures measured in experiment and those estimated by the thermal network model.

In order to limit the meshing level of litz-wire material in the inductor thermal network model, an equivalent longitudinal conductivity k_{leq} is defined (Fig. 12). This k_{leq} is a representation of the faculty for heat to spread longitudinally in the litz wire when the heat comes from its transverse direction. If only transverse and pure longitudinal conductivities (k_t and k_l) are used, a thinner meshing will be required.

There are altogether four different thermal network models, one for each combination of molding height (top and bottom) and layer fill rate (100% and 66%). Fig. 13 shows the thermal network model for samples 1, 2 and 4, which are molded only at the bottom and have 100% layer fill rate. Fig. 14 shows the model for samples 3 and 5, molded to the top with 100% layer fill rate. Thermal network models for samples 6 and 7 are similar to those in Figs. 13 and 14 respectively, but with an additional thermal resistance representing resin in parallel with $R_{\mathrm{litz\_*}}$ to account for the fact that the layer is not full [7].

For each litz-wire sample (#1 to #4), an optimization routine is used to solve the inverse problem of finding the thermal conductivity of the litz wire which minimizes the squared error between the model estimations and the measurements. Fig. 15

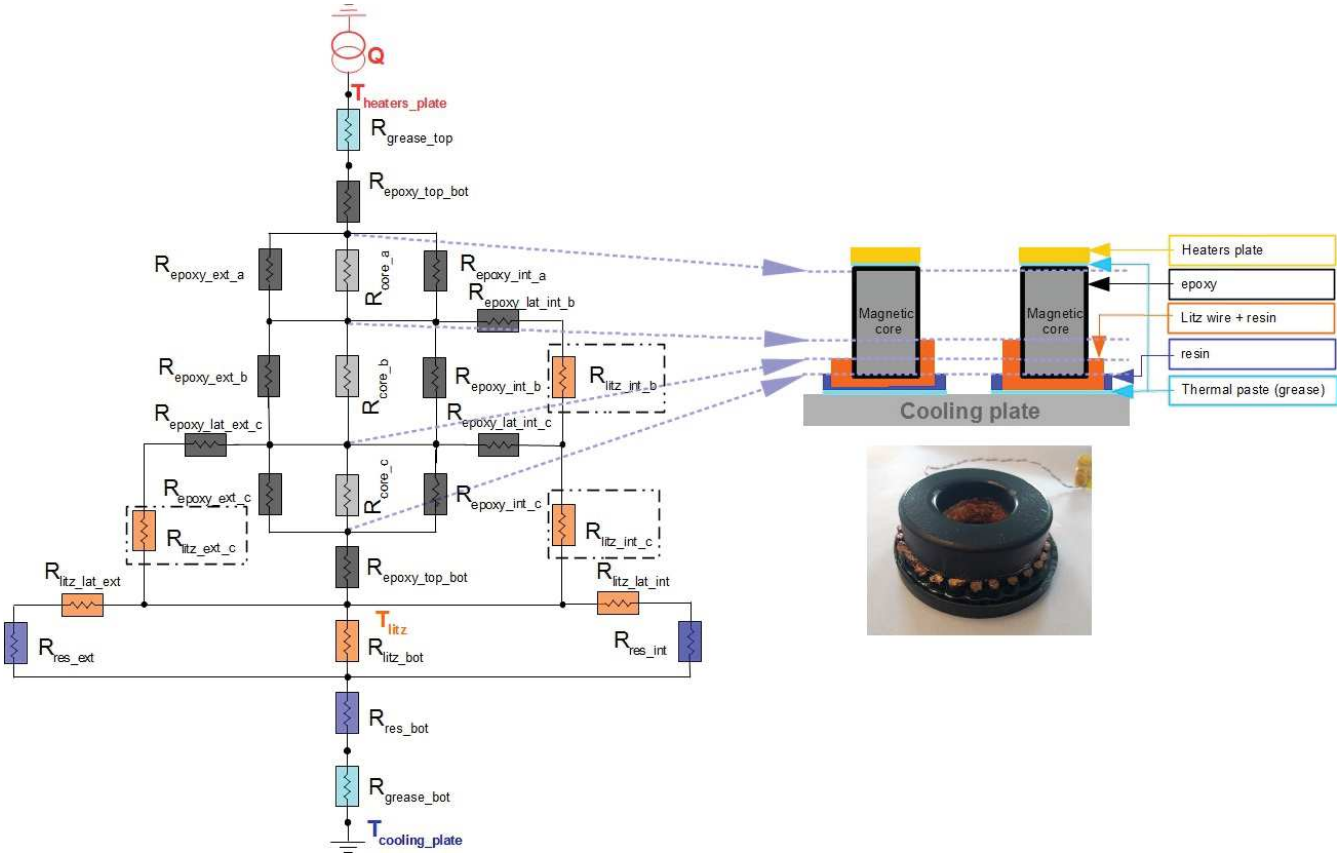

Fig. 13. Thermal network model for samples 1, 2 and 4, showing thermal resistances corresponding to the core material (light grey), epoxy (dark grey), grease (light blue), resin (dark blue) and litz wire (orange). Litz-wire thermal resistances calculated using the equivalent longitudinal conductivity are surrounded by dashed rectangle; the other litz-wire thermal resistances are calculated using the transverse conductivity.

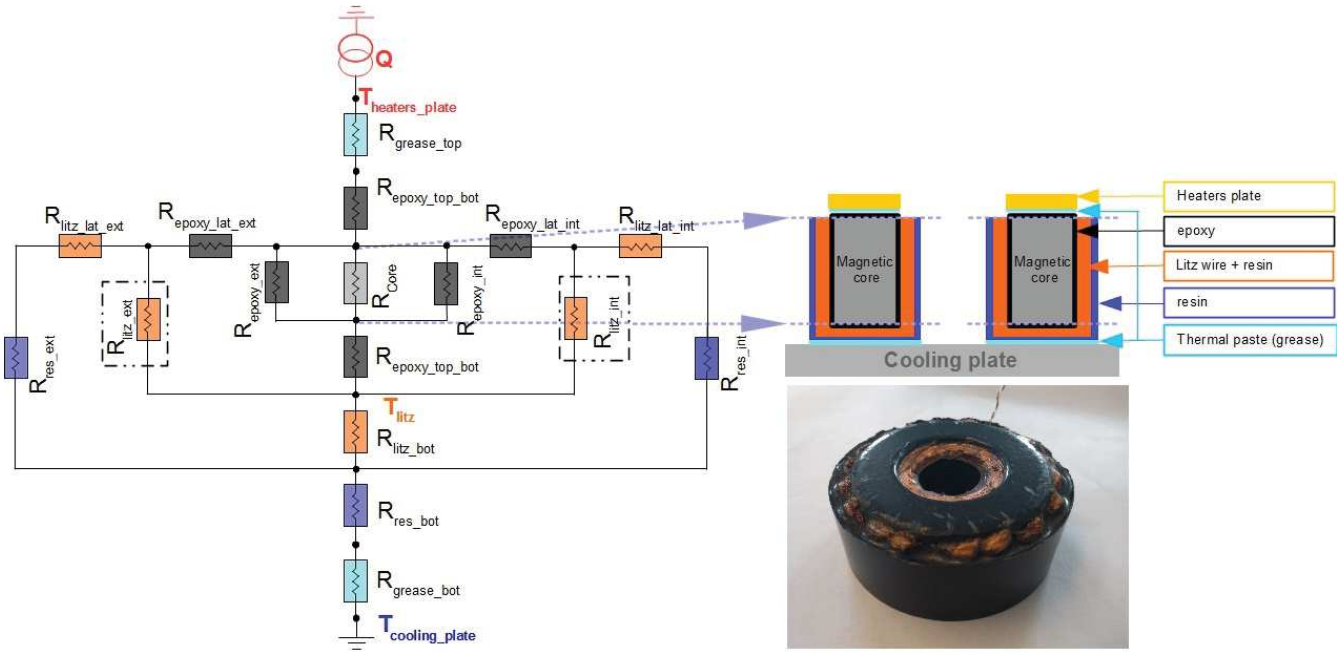

Fig. 14. Thermal network model for samples 3 and 5, showing thermal resistances corresponding to the core material (light grey), epoxy (dark grey), grease (light blue), resin (dark blue) and litz wire (orange). Litz-wire thermal resistances calculated using the equivalent longitudinal conductivity are surrounded by dashed rectangle; the other litz-wire thermal resistances are calculated using the transverse conductivity.

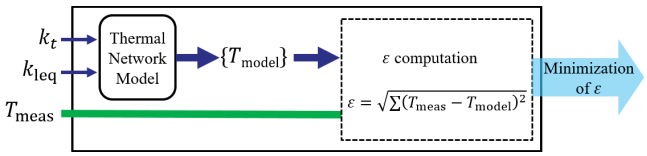

Fig. 15. Inverse problem for calculating the thermal properties of litz wire.

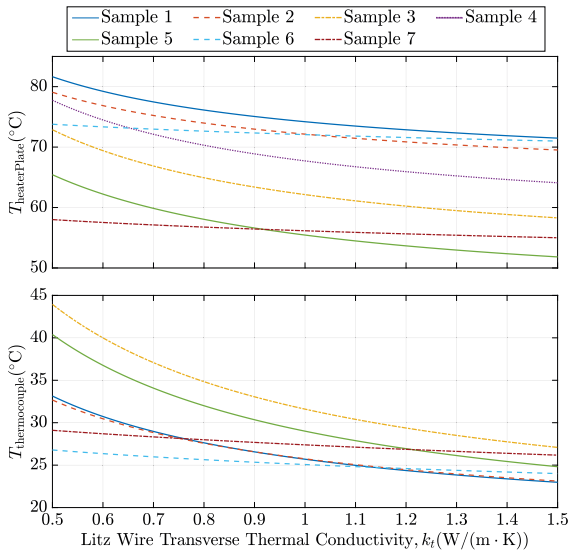

Fig. 16. Hot plate (top) and thermocouple temperatures (bottom) as a function of the transverse thermal conductivity of the litz wire. The temperatures are estimated using the thermal network models shown in Figs. 13 and 14, and similar models for inductor samples 6 and 7.

shows the inverse problem to solve for estimating the litz-wire thermal conductivity. For litz #4, the inverse problem is solved simultaneously for inductor samples 4 to 7. Sensitivity analysis for identifying the litz-wire effective thermal conductivity on various parameters is discussed in [7].

Fig. 16 presents the sensitivity to the litz wire transverse thermal conductivity k_t of the temperature at the hot plate $T_{\text{heaterPlate}}$ and the temperature measured between the bottom of the core and the litz wire $T_{\text{thermocouple}}$. The temperatures were estimated using the thermal network models in Figs. 13 and 14, and similar models for the inductor samples 6 and 7. It shows significant sensitivity of the temperatures to k_t for inductor samples 1–5, all of which have a 100% layer fill rate. The sensitivities of samples 6 and 7, which have a 66% layer fill rate, are poor because of the relatively high thermal conductivity of the epoxy resin potting compared to the litz wire transverse thermal conductivity. Thus, the samples 1 to 5 are more suitable for identification of the transverse thermal conductivity with a low uncertainty.

D. Analytical Model vs. Experimental Identification

The effective transverse thermal conductivities calculated using the proposed analytical model (Section III) are compared to those obtained by optimization from the experimental temperature measurements (Section VI-C). Table V summarizes the values of effective transverse thermal conductivities for each litz wire. The comparison shows that the analytical model and the experimental measurement closely agree with each other, with a maximum error of 12%.

The table also includes both arithmetic and geometric means of the transverse conductivities for square and hexagonal packing. Because the predicted transverse thermal conductivities for the two packings k_t are only different by about 10%, the choice of the particular type of mean does not have a significant impact on the predicted k_t.

The error of the proposed model is less than 2% for litz #1 and #2, and higher for litz #3 and #4. It can be appreciated that litz #1 and #2 are used in inductor samples 1 and 2 respectively, in which the winding is cut and molded only at the bottom of the inductor as shown in Fig. 11 (a); in these samples, the longitudinal thermal conductivity has a negligible impact on the inductor temperatures and the error of the proposed model is very low. Litz #3 is used in the inductor sample 3, which has a molded winding to the top of the inductor core as shown in Fig. 11 (b); the error of the proposed model is larger in this case because the longitudinal thermal conductivity has a larger impact on the inductor temperatures, thereby resulting in a larger uncertainty in the measured thermal conductivity. Litz #4 is used in inductor samples 4–7, with two different layer fill rates and two different molding heights. However, the thermocouple of sample 4 broke during the experiment, sample 5 is molded to the top, and samples 6 and 7 have a 66% layer fill rate. Thus, there is a higher uncertainty in identifying the transverse thermal conductivity from the measured temperatures, which results in a higher error for the proposed model for litz #4.

It should be noted that the error of the proposed model for litz #1 and #2 in Table V are negligible compared to the 10.7% error in the measurement of a brass sample for validating the thermal test bench discussed in Section VI-A. This lower error compared to the test bench validation can be attributed to the low effective thermal conductivity of litz wire, which is about two orders of magnitude lower than that of the brass sample. Thus, similar errors in temperature measurement will result in a much higher error in estimating the thermal conductivity of the brass sample compared to that of litz wire.

For comparison, the transverse thermal conductivity k_t of the four litz wire samples were also calculated using two versions of the TEFA model from [6]. One of the version accounts for the twisting of the litz wire strands (the extended numerical model proposed in [6]), which the other version does not consider (as used in Section IV-B). The results are also included in Table V.

The error of the TEFA model without consideration of the twisting pitch, compared to the experimentally identified litz conductivity, is higher than 50% for each litz wire. This large error can be attributed to the fact that the samples have been molded into a resin having a good thermal conductivity (2.16 $\text{W}/(\text{m} \cdot \text{K})$). This is similar to the result in Fig. 8, which demonstrates that the TEFA model has a larger error for high values of gap thermal conductivity.

The extended version of TEFA model which considers the twisting pitch provides an error less than 18% for litz #2, #3 and #4, compared to less than 12% for the proposed model. This extended version of the TEFA model has a much

TABLE V
TRANSVERSE THERMAL CONDUCTIVITIES, k_t $(\mathrm{W}/(\mathrm{m}\cdot\mathrm{K}))$. THE PERCENTAGE ERRORS ARE SHOWN IN PARENTHESES.

Litz		#1	#2	#3	#4
Experimental		0.79	0.85	1.11	1.225
Proposed Model	Square	0.769	0.813	1.151	1.048
	Hexagonal	0.845	0.891	1.220	1.127
	Arithmetic Mean (Error (%))	0.807 (2.11)	0.852 (0.27)	1.185 (6.79)	1.088 (-11.19)
	Geometric Mean (Error (%))	0.806 (1.99)	0.851 (0.16)	1.185 (6.75)	1.087 (-11.24)
TEFA Model	Without Twisting (Error (%))	0.345 (-56.37)	0.254 (-70.18)	0.327 (-70.56)	0.244 (-80.09)
	With Twisting (Error (%))	1.505 (90.52)	0.899 (5.78)	1.120 (0.89)	1.439 (17.45)

smaller error than the proposed model for litz #3; however, the uncertainty in identifying k_t from the measured temperatures is not negligible due to the impact of longitudinal conductivity. The extended version results in a large error, as much as 90.5% in predicting k_t for litz #1. This large error may be attributed to the short pitch length of litz #1, the small number of strands in each bundle, and the discrete nature of the numerical model of the extended verion of the TEFA model. As the pitch length increases from litz #1 to to #3, the error decreases; the larger error for litz #4 may be attributed to the large uncertainty in identifying the transverse thermal conductivity from the measured temperatures of Samples 5–7.

Thus, it can be concluded that the proposed model can accurately predict the transverse thermal conductivity k_t with an error less than 12%. The error is even smaller if k_t can be more directly identified from the temperature measurements as in the cases of litz #1 and #2. It also provides a smaller range of error compared to the TEFA model of [6].

VII. CONCLUSION

With the growing constraints of integration of power supplies, magnetic components need to be sized considering their environment and available cooling methods. For this purpose, a first-order thermal network model of magnetics is required, in which the main challenge is modeling the thermal properties of the anisotropic litz-wire material; existing models in the literature are not applicable to litz wire, have a large error or require experimental data [4]–[6].

This paper proposed an accurate analytical model of the effective thermal conductivity and resistance of a group of insulated wire strands assuming regular square or hexagonal packing. Comparison of the proposed thermal model to finite element analysis shows a maximum error of 18% for a wide range of parameters. Implementation and application of the proposed model for practical windings and litz-wire strands were also discussed. Experimental identification of litz-wire effective conductivities using some sample inductors also shows that the proposed model agrees closely with the measured results, with an error less than 12%; this error range is less than the error of the benchmark approach.

The proposed model overcomes the limitation of the models found in the literature. The model can be easily implemented to determine effective thermal conductivity of windings or litz wire and can provide insights for improving their thermal performance. The model can also be used by manufacturers for providing data on the effective thermal conductivity of litz wire. Because the model provides a closed-form solution, the computation times are very fast; it takes less than 100 ms to run a thermal network model of the toroidal inductor, together with the proposed model of the winding thermal resistance, on a typical personal computer. It can be used by power electronics designers to fairly and quantitatively compare the performance of many different litz wire designs and potting materials. In other words, the proposed model can be used in an optimization process for magnetics design considering thermal performance.

REFERENCES

[1] J. W. Kolar, D. Bortis, and D. Neumayr, "The ideal switch is not enough," in *Power Semiconductor Devices and ICs (ISPSD), 28th International Symposium on*. IEEE, 2016, pp. 15–22.

[2] C. R. Sullivan, "Prospects for advances in power magnetics," in *Proc. of the 9th International Conference on Integrated Power Electronics Systems (CIPS)*, 2016, pp. 1–9.

[3] M. Delhommais, J.-L. Schanen, F. Wurtz, C. Rigaud, and S. Chardon, "Design by optimization methodology: Application to a wide input and output voltage ranges interleaved buck converter," in *IEEE Energy Conversion Congress and Exposition (ECCE)*, 2017, pp. 3529–3536.

[4] S. Purushothaman and F. de León, "Heat-transfer model for toroidal transformers," *IEEE Transactions on Power Delivery*, vol. 27, no. 2, pp. 813–820, 2012.

[5] R. Wrobel, S. Ayat, and J. L. Baker, "Analytical methods for estimating equivalent thermal conductivity in impregnated electrical windings formed using litz wire," in *IEEE International Electric Machines and Drives Conference (IEMDC)*, 2017, pp. 1–8.

[6] M. Jaritz, A. Hillers, and J. Biela, "General analytical model for the thermal resistance of windings made of solid or litz wire," *IEEE Transactions on Power Electronics*, vol. 34, pp. 668–684, 2019.

[7] M. Delhommais, J.-L. Schanen, F. Wurtz, C. Rigaud, S. Chardon, and S. Vighetti, "Thermal model of litz wire toroidal inductor based on experimental measurements," in *33rd Annual IEEE Applied Power Electronics Conference and Exposition (APEC)*, 2018, pp. 2658–2665.

[8] P. A. Kyaw, J. Qiu, and C. R. Sullivan, "Analytical thermal model for inductor and transformer windings and litz wire," in *IEEE 19th Workshop on Control and Modeling for Power Electronics*, 2018, pp. 1–8.

[9] National Electrical Manufacturers Association, "NEMA standards publication No. MW 1000: Magnet wire," [Online] Available: https://www.nema.org/Products/Pages/MW-1000.aspx, 2016, [Accessed Jul. 5, 2018].

[10] C. R. Sullivan, "Optimal choice for number of strands in a litz-wire transformer winding," *IEEE Transactions on Power Electronics*, vol. 14, no. 2, pp. 283–291, 1999.

[11] I. Vitkauskiene, R. Makuška, U. Stirna, and U. Cabulis, "Thermal properties of polyurethane-polyisocyanurate foams based on poly(ethylene terephthalate) waste," *Medziagotyra*, vol. 17, no. 3, pp. 249–253, 2011.

[12] Fisher Electronik, "Fisher Electronik WLPK 10," [Online] Available: https://www.fischerelektronik.de/web_fischer/en_GB/heatsinks/E01.08/Thermal%20conductive%20paste%C2%A0and%20thermal%20interface%20film/PR/WLPK10/index.xhtml, 2014, [Accessed May. 25, 2018].

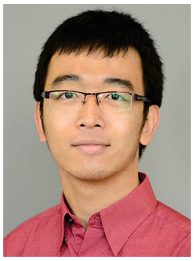

Phyo Aung Kyaw Phyo Aung Kyaw (S'15) received the B.A. degree in physics from the Amherst College, Amherst, MA, USA, in 2014, and the Ph.D. in electrical engineering from Thayer School of Engineering at Dartmouth, Hanover, NH, USA in 2018, where he is currently a postdoctoral research associate. His research interests include power electronics and magnetics, electromagnetic and piezoelectric resonators, high-frequency passive components and wireless power transfer.

Mylène Delhommais (S'18) received the Master degree in electrical engineering from Grenoble Institute of Technology, France, in 2015, and the Ph.D. in electrical engineering from Univ. Grenoble Alpes, France in 2019. Her research activities focus on the optimization methods for the design of power electronics systems.

Jizheng Qiu received the B.E. degree in electronic engineering from Shanghai Jiao Tong University, Shanghai, China, in 2009, and the Ph.D. degree in electrical engineering from Dartmouth College, Hanover, NH, USA, in 2013.

He was with Maxim Integrated, San Jose, CA, USA, as a Senior Member of Technical Staff in high frequency power converters and integrated magnetics designs. He is currently with Tesla, Palo Alto, CA, USA, as a Staff Magnetics Design Engineer in the Power Electronics Team. His current research interests include magnetics design and optimization for power-conversion systems.

Charles R. Sullivan (S'93-M'96-SM'12-F'14) received the B.S.(Hons.) degree in electrical engineering from Princeton University, Princeton, NJ, USA, in 1987, and the Ph.D. degree in electrical engineering from the University of California, Berkeley, CA, USA, in 1996.

Between the B.S. and Ph.D. degrees, he was with Lutron Electronics designing electronic ballasts. He is currently a Professor at Thayer School of Engineering at Dartmouth, Hanover, NH, USA. His research interests include modeling and design optimization of magnetics and other passive components for high-frequency power conversion and wireless power transfer.

Dr. Sullivan received the Power Electronics Society Modeling and Control Technical Achievement Award in 2018 and has received three Power Electronics Society Prize Paper Awards.

Jean-Luc Schanen (M'99SM'04) was born in 1968. He received the Diploma in electrical engineering and the Ph.D. degree from Grenoble Institute of Technology, Grenoble, France, in 1990 and 1994, respectively. He has been a Professor with the Grenoble Institute of Technology since 2003 and is leading the Power Electronics Research Group of the G2ELab. He is also the Deputy Director of the Engineering School of Energy, Water, and Environment. His research activities include the technological design of power electronics systems, including EMC aspects. His group develops models and tools for power converters optimization.

Cécile Rigaud (S'09) received the Master degree in electrical engineering from INSA Strasbourg, France. She is currently a power electronics engineer at Bio-logic Science Instruments where she develops switch-mode power supply based battery testers.